nature geoscience

Article

https://doi.org/10.1038/s41561-025-01649-9

Rapid rise of early ocean pH under elevated weathering rates

Received: 10 April 2024

Accepted: 17 January 2025

Published online: 10 February 2025

Check for updates

Meng Guo [1,2] & Jun Korenaga [2]

Ocean pH is a fundamental property regulating various aspects of Earth system evolution. However, early ocean pH remains controversial, with estimates ranging from strongly acidic to alkaline. Here we develop a model integrating global carbon cycling with ocean geochemistry, and incorporating continental growth and mantle thermal evolution. By coupling global carbon cycle with ocean charge balance, and by using solid Earth processes of mantle degassing and crustal evolution to specify the history of volatile distribution and ocean chemistry, we show that a rapid increase in ocean pH is likely during the Hadean to the early Archaean eons, with pH evolving from 5 to neutral by approximately 4.0 Gyr ago. This rapid pH evolution is attributed primarily to elevated rates of both seafloor and continental weathering during the Hadean. This acceleration in weathering rates originates in the unique aspects of Hadean geodynamics, including rapid crust formation, different crustal lithology and fast plate motion. Earth probably transformed from a hostile state to a habitable one by the end of the Hadean, approximately 4.0 Gyr ago, with important implications for planetary habitability and the origin of life.

Ocean pH regulates carbon partitioning within the hydrosphere, biosynthetic pathways, the stability of crustal and authigenic minerals, and the habitability of Earth. However, early ocean pH remains highly controversial, with estimates ranging from strongly acidic to alkaline[1–6]. Existing ambiguities arise largely from the scarce preservation of Precambrian carbonates, making it difficult to utilize direct proxies, for example, boron isotopes[7], to reconstruct past ocean pH.

Previous efforts have used both empirical and theoretical approaches. Calcium carbonate and sulfate precipitation[8] and high calcium-to-carbonate alkalinity ratios[9] suggest an acidic early ocean, while rare-earth element anomalies in sedimentary rocks argue for a neutral to weakly alkaline pH[10]. The scarcity of gypsum pseudomorphs indicates an early ocean pH of 5.7 to 8.6 (ref. 11), although this could be related to solubility and poor preservation potential. Atmospheric partial pressure of CO_2 (pCO_2) could constrain ocean pH, but its early evolution remains debated[12–17].

Theoretical studies have also yielded varying conclusions, predicting the early ocean to be alkaline[1], acidic[2–4] or approximately neutral[5], due to ambiguities in modelling carbon fluxes. Specifically, the roles of continental and seafloor weathering in balancing the global carbon cycle remain unclear[3–6]. A wide range of continental evolution patterns is adopted[4], spanning rapid early to slow growth, adding uncertainty to continental weathering rates. One longstanding paradigm involves slow and gradual continental growth[18–20], whereas recent studies suggest rapid growth in the Hadean eon[21–26]. Continental growth is, however, not so under-constrained as commonly believed[27]. Additionally, when parameterizing seafloor weathering rate and major ion exchanges between oceans and crusts, previous studies often assume exponentially higher mantle heat flux in the past[3,4,6], inconsistent with petrological estimates on mantle cooling[28]. Therefore, a more justifiable modelling of relevant geochemical cycles, while considering the history of continental formation, becomes imperative.

Considering the above, we developed a model integrating global carbon cycling with ocean geochemistry (Fig. 1), guided by the solid Earth system evolution. Our model explicitly tracks the changing atmospheric pCO_2 and ocean pH using ocean charge balance, incorporating continental growth[23] and mantle thermal evolution[24] to self-consistently constrain the geochemical cycles of carbon, sodium and magnesium.

[1]Asian School of the Environment, Nanyang Technological University, Singapore, Singapore. [2]Department of Earth and Planetary Sciences, Yale University, New Haven, CT, USA. e-mail: meng.guo@ntu.edu.sg

https://doi.org/10.1038/s41561-025-01649-9

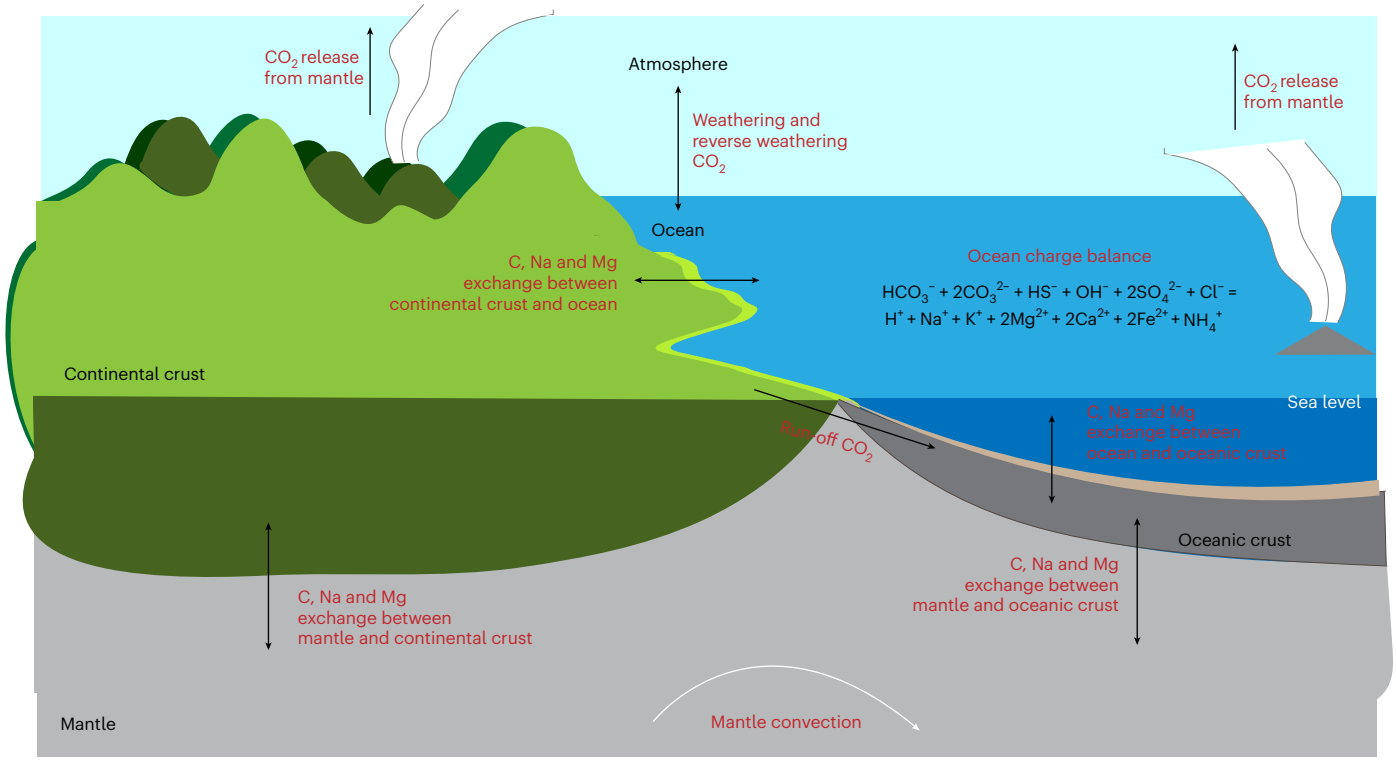

Fig. 1 | Conceptual model of global carbon cycle coupled with ocean chemistry. The history of continental formation and mantle thermal evolution is incorporated to guide the exchange of carbon during mantle degassing, crustal formation, subduction and chemical weathering, as well as the geochemical cycles of sodium and magnesium. The changing atmospheric pCO_2 and ocean pH are tracked throughout Earth history using ocean charge balance.

It also factors in seawater mass changes based on a continental freeboard model[29], which aligns with the modern global water cycle[30,31]. By quantifying carbon exchanges during mantle degassing, crustal formation, subduction and weathering, we map the history of carbon storages and assess the physical mechanisms that lead to the transformation of an initial CO_2-rich atmosphere, expected after magma ocean solidification[32–34], to a habitable one during the early Earth[35].

Here we present an overview of our modelling, summarize results, and discuss the impact of terrestrial and marine silicate weathering on surface conditions. A complete model description is provided in Methods.

We conduct our modelling in three stages using Monte Carlo sampling, similar to ref. 23. First, we simulate various crustal growth models, selecting successful growth models based on the present-day distribution of crustal formation ages[36] (Fig. 2d). Second, the accepted growth models are paired with different thermal evolution models, and such pairs are checked against the Archaean and Proterozoic mantle potential temperatures[28] (Fig. 2e). Lastly, the successful pairs are combined with a global carbon cycle and ocean pH model, where solid Earth evolution controls the rates of carbon subduction, degassing and crustal renewal. The inferred atmospheric pCO_2 values are used to calculate Earth's surface temperature and ocean pH, employing a hybrid atmospheric model and an ocean charge balance model, respectively. The successful solutions at the third stage are chosen based on the present-day and Precambrian pCO_2 levels[13–17], modern ocean pH, surface temperature, seawater ion concentrations[37] and carbon content in terrestrial reservoirs. The successful solutions of seawater ion concentrations are provided in Extended Data Fig. 1.

Our results suggest that surface conditions evolved considerably during the first 500 Myr of Earth history (Fig. 3). Initially, ocean pH was strongly acidic due to the high levels of pCO_2, and the surface temperature could exceed 200 °C. Abundant CO_2 and extreme heat accelerated silicate weathering of both continental and oceanic crusts in the Hadean (Fig. 4a,b), leading to a rapid pCO_2 drop and rising ocean pH. Consequently, the ocean transitioned from acidic to alkaline during the Hadean, with pCO_2 dropping from >100 atm to 10^{-2} atm (Fig. 3). Correspondingly, surface temperature decreased substantially to near 0 °C by the end of the Hadean (Fig. 3).

In our model, the Archaean surface temperature is slightly below present levels, reflecting low luminosity and rapid sequestrations of CO_2. As the early surface temperature is calculated using a one-dimensional (1D) grey atmosphere model without the effects of other greenhouse gases, this low-temperature period does not necessarily indicate a snowball Earth. We also do not account for freezing effects on global carbon cycling, so crossing the freezing point has minimal impact on the model behaviour. Nonetheless, the predicted low surface temperatures around the early Archaean agree with previous theoretical studies[5] and more sophisticated climate simulations[38].

The successful solutions with different starting times of 'reverse weathering'[4,39,40], referring to the consumption of alkalinity and generation of acidity during marine authigenic clay formation, are shown in Fig. 3, and Supplementary Figs. 1 and 2. Reverse weathering, which returns aqueous CO_2 to the atmosphere, causes a sudden increase in pCO_2 and a corresponding decrease in ocean pH. This process has been proposed as a potential solution to the faint young Sun paradox[39]. However, owing to the intense continental and seafloor weathering during the Hadean suggested by our model results, the post-Hadean pCO_2 level remained relatively low (~10^{-2} atm). Additionally, given the large uncertainties in Archaean and Proterozoic pCO_2 estimates[13–17], the exact timing and intensity of reverse weathering could not shift pCO_2 outside the Archaean and Proterozoic constraints and, therefore, does not substantially affect the selection of successful solutions.

The preferred continental evolution models are shown in Fig. 2. While early rapid continental formation is not required in the first two stages (Extended Data Fig. 2), it is favoured by the carbon cycling model to quickly reduce pCO_2 levels on the early Earth, aligning with

https://doi.org/10.1038/s41561-025-01649-9

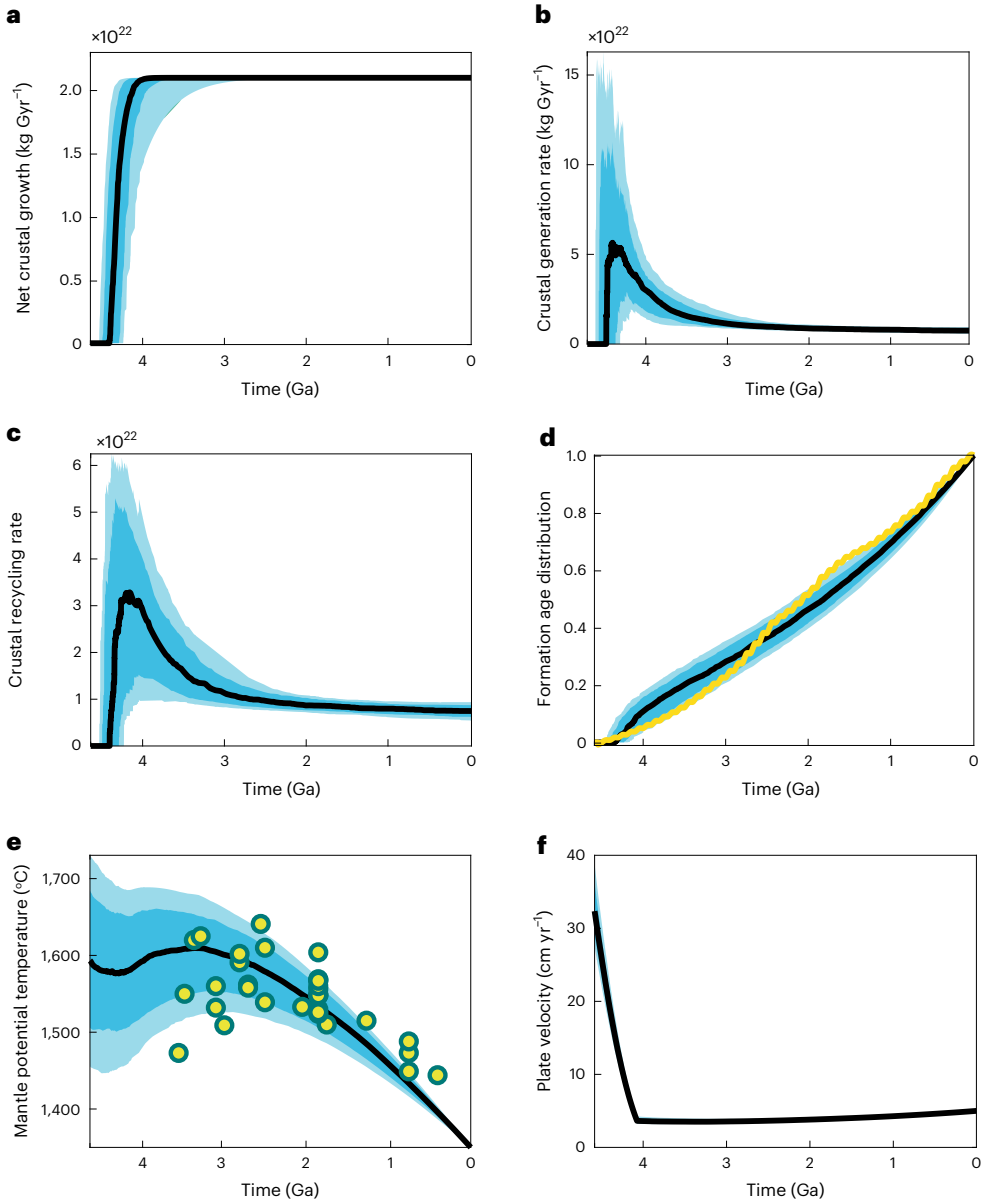

Fig. 2 | Successful solutions with observational constraints. Constraints used to select solutions are shown in yellow. The mid-50% and mid-90% ranges of successful solutions are shown in dark blue and light blue, respectively, with solid lines indicating the medians. A total of 145 successful solutions were analysed. **a**, Net growth of continental crust. **b**, Crustal generation rate. **c**, Crustal recycling rate. **d**, Present-day cumulative distribution of continental formation age. The yellow line is from ref. 36. **e**, Mantle potential temperature. Yellow dots are from ref. 28. **f**, Plate velocity.

Precambrian pCO_2 estimates[13,14]. This results in a continental mass being comparable to the present-day value by the end of the Hadean (Fig. 2a). Meanwhile, all successful solutions show intensive Hadean continental generation (Fig. 2b) and recycling (Fig. 2c), ensuring a steady supply of fresh silicate rock at the surface. Enhanced resurfacing of early crust contributed to the early sequestering of atmospheric CO_2, because the high surface temperatures and pCO_2 levels increased the reactivity of silicate rocks (Fig. 4a).

Our results also indicate that seafloor weathering was probably more influential than continental weathering in producing a clement Earth (Fig. 4a,b). The Hadean seafloor weathering rate is at least one order of magnitude higher compared with its rates during the rest of Earth history, driven by several factors that were probably present during the Hadean, including faster plate velocity (Fig. 2f), elevated pCO_2 levels (Fig. 3a), higher surface temperatures (Fig. 3c) and higher magnesium content (high Mg#) in the oceanic crust produced from a chemically heterogeneous mantle after magma ocean solidification. Modelling of magma ocean solidification suggests that ~75% of the early mantle is occupied by the pyroxenite matrix with an average Mg# of 95 (ref. 41). With the elevated weathering rate, the Hadean oceanic crust sequestered an abundant atmospheric CO_2 (Fig. 4b). Meanwhile, faster plate velocity enabled efficient carbon recycling through subduction (Fig. 4c), aiding early pCO_2 reduction, even with the assumption that only ~50% of subducted carbon is sequestered in the mantle.

As most CO_2 was degassed into the atmosphere during magma ocean solidification[32,33,42], the mantle carbon content was low in the early Hadean (Fig. 5a), reducing carbon degassing through mantle melting. However, fast Hadean plate velocity increased mantle melting rates. These competing effects kept overall mantle carbon degassing relatively steady, with degassing rates only slightly higher in the Hadean (Fig. 4d). Notably, Archaean carbon degassing fluxes are estimated to

https://doi.org/10.1038/s41561-025-01649-9

be 3–8 times the present-day level[43], and our model can reasonably reproduce this trend without using such constraints.

Importance of seafloor weathering on the early Earth

Studies on atmospheric evolution following magma ocean solidification[32,33,42] suggest a dense initial atmosphere with pCO_2 levels of 100–200 atm. The subsequent pCO_2 was primarily controlled by the rates of carbon removal and subduction, considering the relatively low carbon content in the Hadean mantle. Our results suggest that, during the first 500 Myr, the CO_2-rich atmosphere transitioned into a habitable one, the strongly acidic ocean became alkaline and the surface temperature decreased from >200 °C to near 0 °C. These rapid changes were primarily attributed to intense seafloor and continental weathering, driven by high surface temperatures, ample CO_2 supply, rapid formation and destruction of surface rocks, and elevated divalent cations in the crust.

While the role of continental weathering in stabilizing climate is well recognized, the relative importance of seafloor and continental weathering in regulating pCO_2 and global temperatures, along with their overall efficacy in buffering pH, remains controversial[3–5]. In our model, continental weathering became more important than seafloor weathering only by the late Hadean. During the early Hadean (insets in Fig. 4a,b), with high pCO_2, the maximum weathering rates were constrained by the availability of fresh silicate rocks[44,45]. As the compositions of continental and oceanic crusts differ, their maximum capacities of carbon sequestering varied. Assuming complete consumption of major divalent cations (that is, MgO and CaO) in the upper 500 m of the continental crust, Hadean continental weathering consumed only 1.3–1.6 times more CO_2 than today. Based on the restoration model of the upper Archaean continental crust[46], we assume that the maximum continental weathering rate decreased linearly from 1.6 to 1.4 times its present-day level during the Hadean, and subsequently decreased from 1.4 to 1.3 times its present-day level by the end of the Archaean, indicating a modest impact on CO_2 removal. Early Hadean continental weathering was also limited by smaller continental surface area (Figs. 2a and 4a), even though the total continental mass quickly reached the present-day level by the mid-Hadean in our model. Towards the end of the Hadean (~4.0 Gyr ago; Ga), as pCO_2 levels decreased and solar irradiation was low, surface temperatures dropped considerably (Fig. 3c). The Earth's surface temperature directly influences the weathering capability of surface silicate rocks[47], which became the limiting factor for the continental weathering rate in the late Hadean to early Archaean.

In contrast, seafloor weathering may have been more effective than continental weathering in sequestering CO_2 during the early Hadean (Extended Data Fig. 3). The high Mg# in the Hadean oceanic crust, from melting of a chemically heterogeneous mantle, allowed seafloor weathering to consume up to 13 times more CO_2 than today[42]. The frequent renewal of oceanic crust, driven by rapid Hadean plate tectonics, also enhanced seafloor weathering. After the Hadean, the maximum seafloor weathering rate decreased to 6.5 times its present-day level, as oceanic crust composition approached its modern Mg# and plate motion slowed down because mantle chemical heterogeneities were gradually erased by convective mixing. Consequently, the role of seafloor weathering in removing CO_2 became less pronounced compared with continental weathering by the end of the Hadean. Our model, integrating continental evolution, evolving crustal lithology, and mantle thermal and chemical evolution with global carbon cycling, captures this shift in physical mechanisms that stabilized the early climate. Further exploration of the impacts of siliceous life expansion, land plant radiation and continental crust emergence on global carbon cycling would be beneficial. Previous studies on ocean pH evolution suggest that seafloor weathering could effectively buffer the climate against shifts driven by siliceous life expansion[4]; whereas more recent studies indicate a potentially stronger effect of siliceous life expansion[40,48].

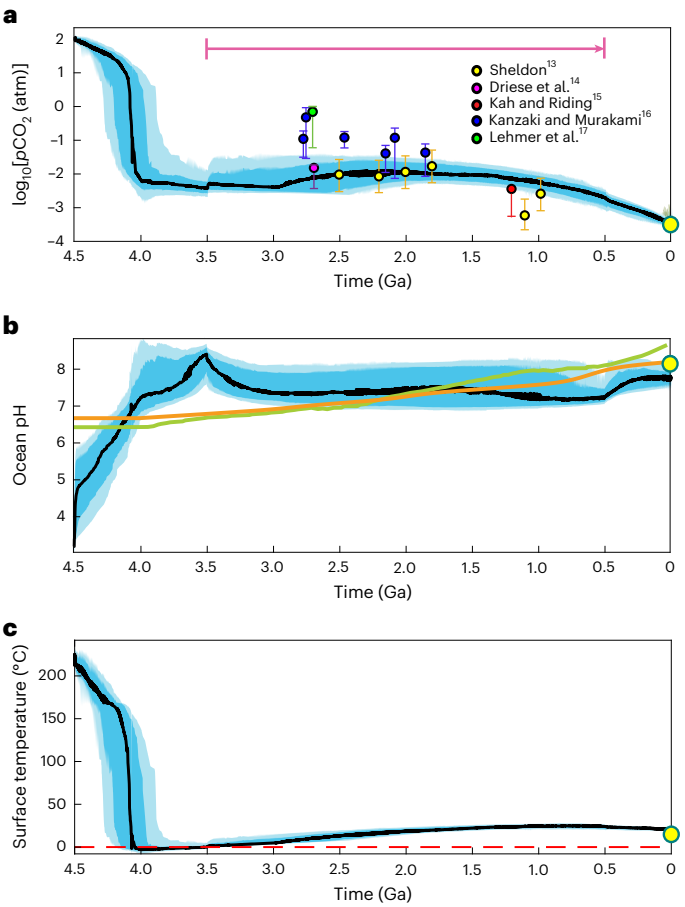

Fig. 3 | Successful solutions and observational constraints of atmospheric pCO_2, ocean pH and surface temperature of Earth, when reverse weathering started 3.5 Ga and turned off 0.5 Ga. Constraints used to select solutions are shown by coloured circles and the error bars represent 2 s.d. The mid-50% and mid-90% ranges of successful solutions are shown in dark blue and light blue, respectively, with solid lines indicating the medians. A total of 145 successful solutions were analysed. **a**, The pCO_2 with proxies from the literature[13–17]. The arrow shows reverse weathering starting 3.5 Ga and turning off 0.5 Ga. **b**, Ocean pH. The median model solutions from ref. 3 and ref. 4 are shown in orange and green lines, respectively. **c**, Earth's surface temperature. The dashed line is drawn at 0 °C.

Implications for the origin of life on the early Earth

The evolution of ocean pH is sensitive to the different modes of crustal growth, and all successful solutions show rapid continental generation and recycling on the early Earth (Fig. 2 and Extended Data Fig. 2). Such continental evolution is necessary to reduce the initial pCO_2 of >100 atm (refs. 32,33,42) to ~10^{-2} atm in the late Archaean to Proterozoic[13,14]. A comparison between solutions with early and late growth of continental crust is shown in Extended Data Fig. 4. After the Hadean, sluggish plate tectonics, constrained by the history of mantle cooling (Fig. 1e,f), limited the weathering capacity of the crust, requiring most carbon sequestration to occur during the Hadean. Thus, our model favours rapid Hadean continental evolution, supporting the notion of substantial continental crust in the Hadean[21–26] and reinforcing the geological basis for Darwin's 'warm little pond' hypothesis of abiogenesis[49].

The extent and timing of early continental emergence, however, still require further investigation. The origin of life traces back to Earth's first two geologic eons, with unequivocal evidence dating back to 3.5 Ga (ref. 50) and possibly extending to 4.1 Ga (ref. 51). Two major abiogenesis hypotheses exist: Darwin's 'warm little pond' theory, suggesting polymerization of organic molecules through wet–dry cycles[49]; and

https://doi.org/10.1038/s41561-025-01649-9

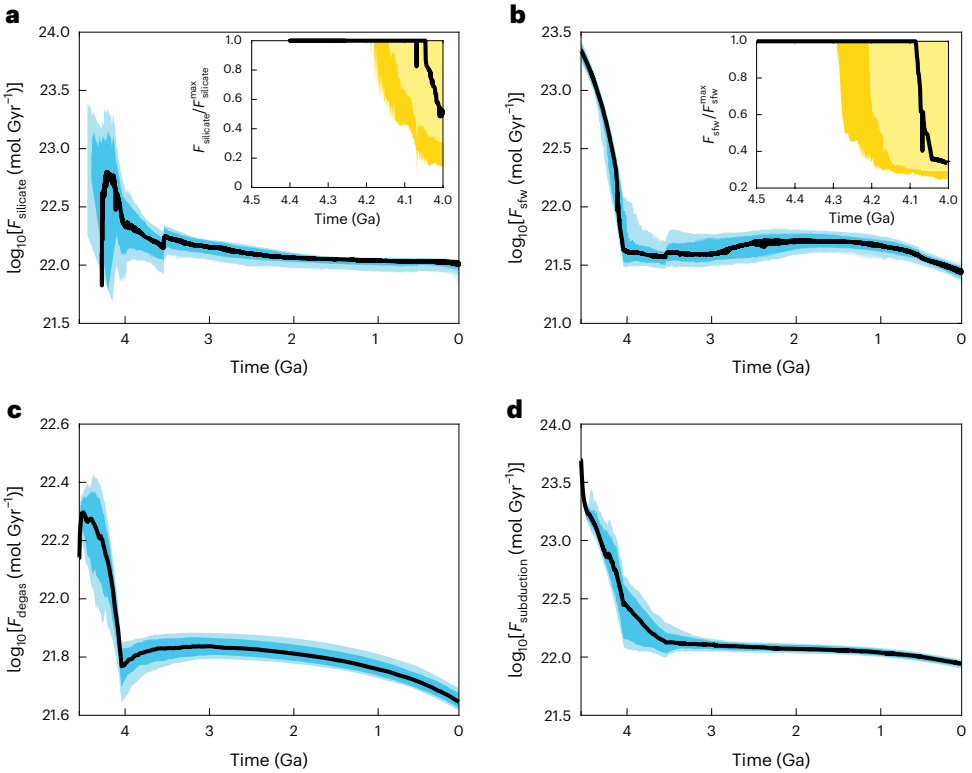

Fig. 4 | Successful solutions for the evolution of carbon fluxes. The mid-50% and mid-90% ranges of successful solutions are shown in dark blue and light blue, respectively, with solid lines indicating the medians. A total of 145 successful solutions were analysed. **a**, Continental silicate weathering ($F_{silicate}$). **b**, Seafloor weathering (F_{sfw}). **c**, Mantle degassing (F_{degas}). **d**, Subduction ($F_{subduction}$). The ratios of maximum silicate weathering potential to actual weathering rates during the Hadean for both continental crust and seafloor are shown as insets in **a** and **b**. In the insets, the mid-50% and mid-90% ranges are shown in light yellow and dark yellow, respectively, with solid lines indicating the medians.

the deep-sea hydrothermal theory[52]. Each of these hypotheses requires specific surface environments; the former necessitates exposed continent and suitable inland water pH, and the latter requires ocean pH favourable for biomolecule formation. Acidic water poses challenges for complex molecule synthesis[53], and atmospheric pCO_2 controls pH in both settings. Our results suggest that pCO_2 decreased to 10^{-2} atm within the Hadean, providing the necessary geological foundation for both hypotheses. The early formation of continental crust was required in lowering the initially high atmospheric pCO_2 and probably facilitated the delivery of growth-limiting nutrients to the surface. By providing constraints on the history of land formation, atmospheric composition and marine chemistry, we delineate a habitability boundary in Earth history to be around the end of the Hadean.

Importance of self-consistent pCO_2 and ocean pH evolution

Compared with Halevy and Bachan[3], our results show a more rapid increase in ocean pH, evolving from ~5 to neutral within the Earth's first 500 Myr. Their model begins with an environment not very different from modern conditions, with a near-neutral ocean pH (6.2–6.5). However, studies on magma ocean solidification[32,33] suggest an initially dense, CO_2-rich atmosphere, implying an initial ocean pH of 3.5–5.5. Solving for this fast CO_2 reduction requires a model that integrates crustal growth, thermal evolution, evolving plate velocities and global carbon cycling. As mentioned earlier, they calculate ocean pH by prescribing pCO_2 evolution (see their Fig. 1b), which essentially determines pH evolution. Also, they do not consider the history of continental growth and the evolving crustal compositions, both of which could impact pH evolution by affecting seawater metal ion concentrations and silicate weathering efficiency. Additionally, their assumption of higher Archaean heat fluxes is inconsistent with petrological estimates of mantle cooling[28]. Mantle heat flux affects seafloor weathering rate and, consequently, chemical exchanges between continental and oceanic crusts in their model. As seafloor weathering rates and seawater cation concentrations decline over time, their model shows a steady pH increase.

On the other hand, Krissansen-Totton et al.[4] employ a pH- and temperature-dependent parameterization for seafloor weathering fluxes and solve for ocean pH using evolving alkalinity and dissolved inorganic carbon in seawater. Their model, like Halevy and Bachan[3], suggests a monotonic increase in ocean pH from 6.5 to 8.2 over Earth history, reaching neutral around 2.5 Ga. They consider various continental growth patterns, but they are biased towards higher heat flow in the past, which, as explained, controls crustal weathering rates and alkalinity exchanges.

Lowering high initial pCO_2 requires substantial CO_2 consumption. Studies on impact ejecta suggest potentially important CO_2 absorption by ejecta weathering[5,6,38]. However, existing studies probably overestimate this effect, by not accounting for carbon re-release due to heating from subsequent impacts. As the mass of impacts decreases exponentially over time, only early impacts can consume a meaningful amount of CO_2 by forming carbonates; however, these carbonates would later release CO_2 due to impact metamorphism if not subducted, especially as early impact events are closely spaced.

Estimates of late Archaean and early Precambrian pCO_2 levels vary widely, from ~0.007 to ~1 atm (refs. 13,14,16,17). As discussed earlier, achieving the late Archaean pCO_2 levels from an initially CO_2-rich atmosphere requires substantial carbon sequestration, enabled by rapid Hadean crustal formation and plate tectonics. After the Hadean, slow plate tectonics (Fig. 2f) and low surface temperatures reduced

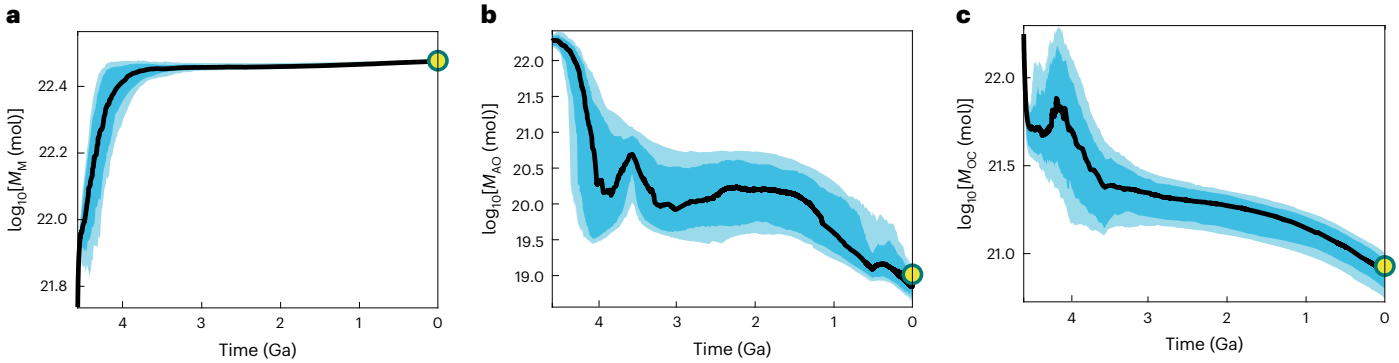

Fig. 5 | Successful solutions for the carbon contents of model reservoirs. The mid-50% and mid-90% ranges of successful solutions are shown in dark blue and light blue, respectively, with solid lines indicating the medians. A total of 145 successful solutions were analysed. Present-day values are shown as yellow dots. **a**, Mantle (M_M). **b**, Atmosphere and oceans (M_{AO}). **c**, Oceanic crust (M_{OC}).

weathering capabilities of both continental and oceanic domains. To reconcile this with the present-day pCO_2, our model favours the lower end of late Archaean and early Proterozoic pCO_2 estimates (Fig. 3a). Owing to limited constraints on reverse weathering, our model only explores reverse weathering rates from zero up to modern levels. Suggested by seawater $\delta^{18}O$ observations[40], a higher-than-modern rate in the Precambrian has been proposed, which could potentially elevate pCO_2. Further investigation into this possibility is warranted.

By integrating Earth interior processes with the history of volatile distribution and ocean chemistry, we present a plausible scenario for Earth's transformation from a hostile to a habitable state during the Hadean. Our model represents an attempt to incorporate continental evolution, changing crustal lithology, and mantle thermal evolution in a self-consistent global carbon cycle framework, enabling a more accurate assessment of climate feedback from continental and seafloor weathering. As the early ocean pH controlled the solubility, speciation and bioavailability of key nutrients, understanding its evolution lays the groundwork for future studies on the origin of life.

Online content

Any methods, additional references, Nature Portfolio reporting summaries, source data, extended data, supplementary information, acknowledgements, peer review information; details of author contributions and competing interests; and statements of data and code availability are available at https://doi.org/10.1038/s41561-025-01649-9.

References

1. Kempe, S. & Degens, E. T. An early soda ocean? *Chem. Geol.* **53**, 95–108 (1985).
2. Macleod, G., McKeown, C., Hall, A. J. & Russell, M. J. Hydrothermal and oceanic pH conditions of possible relevance to the origin of life. *Origins Life Evol. Biosphere* **24**, 19–41 (1994).
3. Halevy, I. & Bachan, A. The geologic history of seawater pH. *Science* **355**, 1069–1071 (2017).
4. Krissansen-Totton, J., Arney, G. N. & Catling, D. C. Constraining the climate and ocean pH of the early Earth with a geological carbon cycle model. *Proc. Natl Acad. Sci. USA* **115**, 4105–4110 (2018).
5. Sleep, N. H. & Zahnle, K. Carbon dioxide cycling and implications for climate on ancient Earth. *J. Geophys. Res. Planets* **106**, 1373–1399 (2001).
6. Kadoya, S., Krissansen-Totton, J. & Catling, D. C. Probable cold and alkaline surface environment of the Hadean Earth caused by impact ejecta weathering. *Geochem. Geophys. Geosyst.* **21**, e2019GC008734 (2020).
7. Pagani, M., Zachos, J. C., Freeman, K. H., Tipple, B. & Bohaty, S. Marked decline in atmospheric carbon dioxide concentrations during the Paleogene. *Science* **309**, 600–603 (2005).
8. Walker, J. C. Possible limits on the composition of the Archaean ocean. *Nature* **302**, 518–520 (1983).
9. Blättler, C. L. et al. Constraints on ocean carbonate chemistry and pCO_2 in the Archaean and Palaeoproterozoic. *Nat. Geosci.* **10**, 41–45 (2017).
10. Friend, C. R., Nutman, A. P., Bennett, V. C. & Norman, M. D. Seawater-like trace element signatures (REE + Y) of Eoarchaean chemical sedimentary rocks from southern West Greenland, and their corruption during high-grade metamorphism. *Contrib. Mineral. Petrol.* **155**, 229–246 (2008).
11. Retallack, G. J. & Schmitz, M. D. Archean (3.3 Ga) paleosols and paleoenvironments of Western Australia. *PLoS One* **18**, e0291074 (2023).
12. Kasting, J. F. Theoretical constraints on oxygen and carbon dioxide concentrations in the Precambrian atmosphere. *Precambrian Res.* **34**, 205–229 (1987).
13. Sheldon, N. D. Precambrian paleosols and atmospheric CO_2 levels. *Precambrian Res.* **147**, 148–155 (2006).
14. Driese, S. G. et al. Neoarchean paleoweathering of tonalite and metabasalt: implications for reconstructions of 2.69 Ga early terrestrial ecosystems and paleoatmospheric chemistry. *Precambrian Res.* **189**, 1–17 (2011).
15. Kah, L. C. & Riding, R. Mesoproterozoic carbon dioxide levels inferred from calcified cyanobacteria. *Geology* **35**, 799–802 (2007).
16. Kanzaki, Y. & Murakami, T. Estimates of atmospheric CO_2 in the Neoarchean–Paleoproterozoic from paleosols. *Geochim. Cosmochim. Acta* **159**, 190–219 (2015).
17. Lehmer, O. R., Catling, D. C., Buick, R., Brownlee, D. E. & Newport, S. Atmospheric CO_2 levels from 2.7 billion years ago inferred from micrometeorite oxidation. *Sci. Adv.* **6**, eaay4644 (2020).
18. McLennan, S. M. & Taylor, S. R. Geochemical constraints on the growth of the continental crust. *J. Geol.* **90**, 347–361 (1982).
19. Campbell, I. H. Constraints on continental growth models from Nb/U ratios in the 3.5 Ga Barberton and other Archaean basalt-komatiite suites. *Am. J. Sci.* **303**, 319–351 (2003).
20. Cawood, P. A. et al. Secular evolution of continents and the Earth system. *Rev. Geophys.* **60**, e2022RG000789 (2022).
21. Keller, B. & Schoene, B. Plate tectonics and continental basaltic geochemistry throughout Earth history. *Earth Planet. Sci. Lett.* **481**, 290–304 (2018).
22. McCoy-West, A. J. et al. Extensive crustal extraction in Earth's early history inferred from molybdenum isotopes. *Nat. Geosci.* **12**, 946–951 (2019).
23. Guo, M. & Korenaga, J. Argon constraints on the early growth of felsic continental crust. *Sci. Adv.* **6**, eaaz6234 (2020).

24. Guo, M. & Korenaga, J. The combined Hf and Nd isotope evolution of the depleted mantle requires Hadean continental formation. *Sci. Adv.* **9**, eade2711 (2023).
25. Korenaga, J. Crustal evolution and mantle dynamics through Earth history. *Phil. Trans. R. Soc. A* **376**, 20170408 (2018).
26. Jiang, J. et al. Sediment subduction in Hadean revealed by machine learning. *Proc. Natl Acad. Sci. USA* **121**, e2405160121 (2024).
27. Korenaga, J. & Spencer, C. J. in *Treatise on Geochemistry* 3rd edn (ed. Chauvel, C.) Vol. 2, 699–727 (Elsevier Inc., 2025).
28. Herzberg, C., Condie, K. & Korenaga, J. Thermal history of the Earth and its petrological expression. *Earth Planet. Sci. Lett.* **292**, 79–88 (2010).
29. Korenaga, J., Planavsky, N. J. & Evans, D. A. D. Global water cycle and the coevolution of Earth's interior and surface environment. *Phil. Trans. R. Soc. A* **375**, 20150393 (2017).
30. Ito, E., Harris, D. M. & Anderson, A. T. Jr Alteration of oceanic crust and geologic cycling of chlorine and water. *Geochim. Cosmochim. Acta* **47**, 1613–1624 (1983).
31. Jarrard, R. D. Subduction fluxes of water, carbon dioxide, chlorine, and potassium. *Geochem. Geophys. Geosyst.* **4**, 8905 (2003).
32. Abe, Y. Physical state of the very early Earth. *Lithos* **30**, 223–235 (1993).
33. Zahnle, K. et al. Emergence of a habitable planet. *Space Sci. Rev.* **129**, 35–78 (2007).
34. Sossi, P. A. et al. Redox state of Earth's magma ocean and its Venus-like early atmosphere. *Sci. Adv.* **6**, eabd1387 (2020).
35. Catling, D. C. & Zahnle, K. J. The Archean atmosphere. *Sci. Adv.* **6**, eaax1420 (2020).
36. Korenaga, J. Estimating the formation age distribution of continental crust by unmixing zircon ages. *Earth Planet. Sci. Lett.* **482**, 388–395 (2018).
37. Dickson, A. G. & Goyet, C. (eds) *Handbook of Methods for the Analysis of the Various Parameters of the Carbon Dioxide System in Sea Water* Version 2 (DOE, 1994).
38. Charnay, B., Le Hir, G., Fluteau, F., Forget, F. & Catling, D. C. A warm or a cold early Earth? New insights from a 3-D climate–carbon model. *Earth Planet. Sci. Lett.* **474**, 97–109 (2017).
39. Isson, T. T. & Planavsky, N. J. Reverse weathering as a long-term stabilizer of marine pH and planetary climate. *Nature* **560**, 471–475 (2018).
40. Isson, T. & Rauzi, S. Oxygen isotope ensemble reveals Earth's seawater, temperature, and carbon cycle history. *Science* **383**, 666–670 (2024).
41. Miyazaki, Y. & Korenaga, J. On the timescale of magma ocean solidification and its chemical consequences: 2. Compositional differentiation under crystal accumulation and matrix compaction. *J. Geophys. Res. Solid Earth* **124**, 3399–3419 (2019).
42. Miyazaki, Y. & Korenaga, J. A wet heterogeneous mantle creates a habitable world in the Hadean. *Nature* **603**, 86–90 (2022).
43. Des Marais, D. J. in *The Carbon Cycle and Atmospheric CO_2: Natural Variations Archean to Present* (eds Sundquist, E. T. & Broecker, W. S.) 602–611, Geophysical Monograph 32 (American Geophysical Union, 1985).
44. West, A. J., Galy, A. & Bickle, M. Tectonic and climatic controls on silicate weathering. *Earth Planet. Sci. Lett.* **235**, 211–228 (2005).
45. Foley, B. J. The role of plate tectonic–climate coupling and exposed land area in the development of habitable climates on rocky planets. *Astrophys. J.* **812**, 36 (2015).
46. Condie, K. C. Chemical composition and evolution of the upper continental crust: contrasting results from surface samples and shales. *Chem. Geol.* **104**, 1–37 (1993).
47. Walker, J. C., Hays, P. B. & Kasting, J. F. A negative feedback mechanism for the long-term stabilization of Earth's surface temperature. *J. Geophys. Res. Oceans* **86**, 9776–9782 (1981).
48. Sharoni, S. & Halevy, I. Rates of seafloor and continental weathering govern Phanerozoic marine phosphate levels. *Nat. Geosci.* **16**, 75–81 (2023).
49. Damer, B. A field trip to the Archaean in search of Darwin's warm little pond. *Life* **6**, 21 (2016).
50. Walter, M. R., Buick, R. & Dunlop, J. S. R. Stromatolites 3,400–3,500 Myr old from the North Pole area, Western Australia. *Nature* **284**, 443–445 (1980).
51. Bell, E. A., Boehnke, P., Harrison, T. M. & Mao, W. L. Potentially biogenic carbon preserved in a 4.1 billion-year-old zircon. *Proc. Natl Acad. Sci. USA* **112**, 14518–14521 (2015).
52. Russell, M. J. et al. The drive to life on wet and icy worlds. *Astrobiology* **14**, 308–343 (2014).
53. Benner, S. A., Kim, H. J., Kim, M. J. & Ricardo, A. Planetary organic chemistry and the origins of biomolecules. *Cold Spring Harb. Perspect. Biol.* **2**, a003467 (2010).

Methods

We developed a global carbon cycle model coupled with ocean charge balance to explore the co-evolution of atmospheric CO_2 and seawater acidity. The model integrates crust, mantle, atmosphere and ocean interactions, using mantle thermal evolution and Earth's surface processes to track volatile and incompatible element distribution across reservoirs.

The mantle's thermal evolution and continental formation history drive changes in the global carbon cycle, parameterized based on refs. 23,24. The mantle heat flux (Q) has been adjusted to reflect updated insights regarding Hadean mantle conditions. Rapid plate tectonics in the Hadean is essential to sequester the massive amount of atmospheric carbon resulting from magma ocean solidification, as it has long been speculated in the literature[5,33,54]. Rapid plate movement is possible in the Hadean if magma ocean solidification results in a wet, chemically heterogeneous mantle[42], which is currently the only physically plausible mechanism that can enable this process. Owing to different lithologies, melting of a heterogeneous mantle wouldn't form a thick depleted lithosphere even at high temperatures, enabling rapid tectonics. Following ref. 42, Q is set to be three times its current value initially (a tenfold increase in plate velocity) and decreases linearly to the Archaean value due to convective mixing. From the Archaean to present, Q is held constant at 36 TW, aligning with petrological estimates of mantle thermal evolution[28] as well as geochemical models of Earth's composition. Such a constant heat flux over time corresponds to more sluggish plate tectonics in the past[55]. A hybrid atmospheric model is used to determine the surface temperatures under different solar irradiation and atmospheric pCO_2.

We conduct our modelling in three stages, first with crustal evolution only, then with thermal evolution, and finally with global carbon cycle and ocean pH, using Monte Carlo sampling throughout. Successful models from the first two stages, filtered by present-day continental formation age distribution[36] and the Archaean and Proterozoic mantle temperatures[28], are used to calculate atmospheric pCO_2 and ocean pH evolution. Final successful results are constrained by present-day and Precambrian pCO_2 levels[13–17], present-day ocean pH (8.2), surface temperature (12 °C), concentrations of major seawater ions[37], and carbon content in the atmosphere (3.9×10^{16} mol), oceans (3.6×10^{18} mol), oceanic crust (8.5×10^{20} mol), and mantle (3×10^{22} mol).

In the following sections, we describe the global carbon cycle model, the ocean charge balance model and the hybrid atmospheric model.

The global carbon cycle model

Parameterization of carbon fluxes. We consider four major reservoirs in the global carbon cycle model: mantle, continental crust, oceanic crust, and the combined reservoir of atmosphere and oceans (Fig. 1). The atmosphere and oceans are treated as a single reservoir due to CO_2 solubility equilibrium[4,5]. We assume that the carbon content in the continental crust is proportional to its mass, as it grows through accretion and erodes via subduction[4,5,45,56].

The following governing equations describe how carbon is added and removed from reservoirs of oceanic plates (M_{OC}), atmosphere and ocean (M_{AO}), and mantle (M_M) through geological processes[5,45,56,57]:

$$\frac{dM_{OC}(t)}{dt} = \frac{F_{silicate}(t)}{2} + F_{sfw}(t) - F_{sub}(t), \quad (1)$$

$$\frac{dM_{AO}(t)}{dt} = F_{degas}(t) + fF_{sub}(t) - \frac{F_{silicate}(t)}{2} - F_{sfw}(t) - F_{CC}(t) - F_{osub}(t), \quad (2)$$

$$\frac{dM_M(t)}{dt} = (1-f)F_{sub}(t) + F_{osub}(t) - F_{degas}(t), \quad (3)$$

where M represents reservoir sizes, t is time, F represents various carbon fluxes, and f is a factor that accounts for incomplete degassing at subduction zones, with a mean value of 0.5 and a standard deviation of ±0.1 (ref. 58). Note that the carbon content in the continental crust (M_{CC}) is assumed to be proportional to its mass evolution throughout Earth history (Ms_{CC}) ($M_{CC}(t) = M_{CC}(t_p)\,Ms_{CC}(t)/Ms_{CC}(t_p)$) and the amount of carbon deposited on continental crust from the ocean is denoted by F_{CC}, which represents the change in M_{CC}.

The term $F_{silicate}$ is the carbon flux from atmosphere to oceanic plates due to continental silicate weathering, which is divided by two in equation (1), because only half of the carbon initially sequestered during silicate weathering can be stored within oceanic plates[59]. We model the temporal variation of $F_{silicate}$ as[56]:

$$F_{silicate}(t) = F^*_{silicate}(t) f_{land}(t) \frac{\dot{M}_u(t)}{\dot{M}_u(t_p)}, \quad (4)$$

where f_{land} is the ratio of the exposed weatherable land area to present-day area, which is assumed to be proportional to the ratio of the mass of continental crust at a given time to its present-day mass; and $\dot{M}_u$ is the generation rate of continental crust[23]. We model the continental crust evolution following ref. 23. The term $F^*_{silicate}$ denotes a weathering function[47,56,59,60]:

$$F^*_{silicate}(t) = F_{silicate}(t_p)\left(\frac{pCO_2(t)}{pCO_2(t_p)}\right)^{0.55}\left(\frac{P_{sat}(t)}{P_{sat}(t_p)}\right)^{0.3} \exp\left(\frac{E_a}{R_g}\left(\frac{1}{T(t_p)} - \frac{1}{T(t)}\right)\right). \quad (5)$$

where the term t_p represents the present day, E_a is the activation energy (4.186×10^4 J mol^{-1}; ref. 60), R_g is the gas constant (8.314 J K^{-1} mol^{-1}) and $T(t_p)$ is the reference temperature (298 K). In equation (5), $F_{silicate}(t_p)$ is the present-day silicate weathering flux[61–64], the second term describes the influence of the partial pressure of atmospheric CO_2, the third term denotes the influence of precipitation and run-off, and the last term is the influence of temperature on continental silicate weathering. The term P_{sat} denotes the saturation pressure[65]:

$$P_{sat}(t) = P^*_{sat}\exp\left(\frac{m_w L_w}{R_g}\left(\frac{1}{T^*} - \frac{1}{T(t)}\right)\right), \quad (6)$$

where P^*_{sat} (610 Pa) is the reference saturation vapour pressure at the reference temperature T^* (273 K), m_w is the molar mass of water (18 g mol^{-1}) and L_w is the latent heat of water (2,469 J g^{-1}). The surface temperature, T, is calculated in the hybrid atmospheric model ('A hybrid atmospheric model').

For most of Earth history, equation (5) can describe the weathering reaction kinetics between CO_2 and silicate rocks. However, during the Hadean to the early Archaean, when atmospheric CO_2 is abundant, the maximum rate of terrestrial silicate weathering ($F^{max}_{silicate}$) is capped by the availability of fresh rocks[44,45], controlled by the generation rate and composition of continental crust. Thus, we define $F^{max}_{silicate}$ as the CO_2 sequestered in the uppermost 500 m of the continental crust[66] multiplied by its generation rate, assuming complete consumption of oxide components, MgO, CaO, Na_2O and K_2O, to form carbonates. To account for changing crustal lithology, we use oxide compositions for Hadean and Archaean upper crusts based on a restoration model for continental crust older than 3.5 Gyr and between 3.5 and 2.5 Gyr, respectively[46].

The term F_{sfw} is the carbon flux from oceans to oceanic plates resulting from seafloor hydrothermal alteration. It should be noted that F_{sfw} only includes the alteration of basalt by CO_2 dissolved in the oceans; formation of carbonates by calcium and bicarbonate ions derived from continental silicate weathering are accounted by $F_{silicate}$. We model F_{sfw} as follows:

$$F_{sfw}(t) = F_{sfw}(t_p)\left(\frac{v(t)}{v(t_p)}\right)\left(\frac{pCO_2(t)}{pCO_2(t_p)}\right)^{0.25}, \quad (7)$$

where the first term ($F_{sfw}(t_p)$) is the present-day seafloor weathering flux[48,67]; the second and the last term denote the influences of plate velocity and atmospheric CO_2 partial pressure on seafloor weathering, respectively. The exponential dependence of F_{sfw} on pCO_2 is set to be 0.25 (refs. 45,68) and the present-day atmospheric CO_2 partial pressure ($pCO_2(t_p)$) is set to 33 Pa (ref. 65).

Similar to $F^{max}_{silicate}$, we define the maximum seafloor weathering rate (F^{max}_{sfw}) as the amount of CO_2 sequestered in the uppermost 500 m of the oceanic crust[69,70] multiplied by plate velocity, assuming complete alteration of MgO and CaO into carbonates. With the present-day oceanic crust composition, F^{max}_{sfw} can be 6.5 times the present-day seafloor weathering rate. During the Hadean, when oceanic crust was probably ultramafic due to melting of the high Mg# matrix in the mantle[42] (Supplementary Table 2), F^{max}_{sfw} is assumed to decrease linearly from 13 times to 6.5 times the modern rate. Plate velocity is calculated based on mantle thermal evolution[28] with an initial value 10 times higher, tapering to the Archaean rate by the end of the Hadean.

The term F_{osub} is the carbon flux lost from ocean to mantle during subduction, which is calculated as:

$$F_{osub}(t) = \frac{M_{ocean}(t-1)(Ms_{ocean}(t) - Ms_{ocean}(t-1))}{Ms_{ocean}(t-1)}, \quad (8)$$

where M_{ocean} represents inorganic carbon in the ocean and Ms_{ocean} is the ocean mass. The initial ocean mass, $Ms_{ocean}(t_0)$, is assumed to be in the range of 10–40% of the present-day value[42]. It linearly increases to 200–300% of the present-day value by the end of the Hadean, $Ms_{ocean}(t_{4.0})$, and then linearly decreases to the present-day value, $Ms_{ocean}(t_p)$, during the rest of Earth history. Thus, during the Hadean, the mass evolution of the oceans can be expressed as $Ms_{ocean}(t) = Ms_{ocean}(t_0) + (Ms_{ocean}(t_{4.0}) - Ms_{ocean}(t_0))(t - t_0)/(t_{4.0} - t_0)$; whereas for the rest of Earth history, $Ms_{ocean}(t) = Ms_{ocean}(t_{4.0}) + (Ms_{ocean}(t_p) - Ms_{ocean}(t_{4.0}))(t_p - t_{4.0})/(t - t_{4.0})$.

The term F_{sub} is the carbon flux by the subducted oceanic plates, which can be expressed as:

$$F_{sub}(t) = F_{sub}(t_p)\frac{v(t)}{v(t_p)}\frac{M_{OC}(t)}{M_{OC}(t_p)}, \quad (9)$$

where $F_{sub}(t_p)$ is the present-day subducted carbon flux (1–15 × 10^{12} mol yr^{-1}; refs. 31,71,72). The term f in equations (2) and (3) denotes the fraction of carbon that is degassed through arc volcanism before reaching the mantle, which is set to be 0.5. Thus, the term fF_{sub} represents the carbon flux released back to the atmosphere and ocean via arc volcanism and $(1-f)F_{sub}$ denotes the carbon flux that is recycled back into the mantle.

The term F_{degas} is the carbon flux degassed from the mantle to the atmosphere through mid-ocean ridge volcanism, which is influenced by the carbon content in the mantle (M_M), plate velocity (v) and mantle melting depth (z) as:

$$F_{degas}(t) = F_{degas}(t_p)\frac{M_M(t)}{M_M(t_p)}\frac{v(t)}{v(t_p)}\frac{z(t)}{z(t_p)}, \quad (10)$$

where $F_{degas}(t_p)$ is the present-day mantle outgassing flux (1–10 × 10^{12} mol yr^{-1}; refs. 73,74).

Parameterization of carbon reservoir sizes. In the atmosphere, pCO_2 is defined as following:

$$pCO_2(t) = \frac{M_{atm}(t)m_{CO_2}g}{A_{earth}}, \quad (11)$$

where M_{atm} is the atmospheric carbon abundance, A_{earth} is the surface area of the Earth (5.1×10^{14} km^2), g is the acceleration of gravity (9.8 m s^{-1}) and m_{CO_2} is the molar mass of CO_2 (44 g mol^{-1}). Rearranging equation (11), M_{atm} can be expressed with pCO_2 as the following:

$$M_{atm}(t) = \frac{pCO_2(t)A_{earth}}{m_{CO_2}g}. \quad (12)$$

At the same time, the abundance of inorganic carbon in the ocean (M_{ocean}) can be calculated as:

$$M_{ocean} = [CO_2]_{aq} + [HCO_3^-] + [CO_3^{2-}], \quad (13)$$

where $[CO_2]_{aq}$, $[HCO_3^-]$ and $[CO_3^{2-}]$ are the concentrations of dissolved CO_2, HCO_3^- and CO_3^{2-} in the oceans, respectively. These concentrations can be related to pCO_2 through equilibrium constants:

$$M_{ocean}(t) = \left(pCO_2(t)K_H + \frac{pCO_2(t)K_HK_{A1}}{[H^+]} + \frac{pCO_2(t)K_HK_{A1}K_{A2}}{[H^+]^2}\right)Ms_{ocean}(t), \quad (14)$$

where K_H, K_{A1} and K_{A2} are Henry's law constant, the first dissociation constant of carbonic acid and the second dissociation constant of carbonic acid, respectively (Supplementary Table 1); $[H^+]$ is the concentration of hydrogen ions in the oceans; and Ms_{ocean} is the mass of the oceans.

The combined carbon reservoir of the atmosphere and oceans (M_{AO}) can be expressed as:

$$M_{AO}(t) = M_{atm}(t) + M_{ocean}(t). \quad (15)$$

Thus, M_{AO} can be calculated using pCO_2 and $[H^+]$ as follows:

$$M_{AO}(t) = pCO_2(t)\left(\left(K_H + \frac{K_HK_{A1}}{[H^+]} + \frac{K_HK_{A1}K_{A2}}{[H^+]^2}\right)Ms_{ocean}(t) + \frac{A_{earth}}{m_{CO_2}g}\right). \quad (16)$$

The ocean charge balance model

Following Halevy and Bachan[3], we consider the concentrations of the following major ions for ocean charge balance:

$$[HCO_3^-] + 2[CO_3^{2-}] + [HS^-] + [OH^-] + 2[SO_4^{2-}] + [Cl^-] = [H^+] + [Na^+] + [K^+] + 2[Mg^{2+}] + 2[Ca^{2+}] + 2[Fe^{2+}] + [NH_4^+]. \quad (17)$$

Among these ions, the concentration of $[HCO_3^-]$, $[CO_3^{2-}]$, $[OH^-]$ and $[Ca^{2+}]$ can be expressed with pCO_2, $[H^+]$ and relevant equilibrium constants:

$$\begin{aligned} &pCO_2K_HK_{A1}[H^+] + 2pCO_2K_HK_{A1}K_{A2} + [HS^-][H^+]^2 \\ &+ K_W[H^+] + 2[SO_4^{2-}][H^+]^2 + [Cl^-][H^+]^2 \\ &= [H^+]^3 + [Na^+][H^+]^2 + [K^+][H^+]^2 + 2[Mg^{2+}][H^+]^2 \\ &+ \frac{2n_{sat}K_{SP}[H^+]^4}{pCO_2K_HK_{A1}K_{A2}} + 2[Fe^{2+}][H^+]^2 + [NH_4^+][H^+]^2, \end{aligned} \quad (18)$$

where K_W and K_{SP} (4.2658×10^{-7}) are the water dissociation constant and calcite solubility product constant, respectively, and n_{sat} is the calcite saturation factor[3].

The evolving concentrations of $[Na^+]$ and $[Mg^{2+}]$ in seawater are explicitly modelled according to their respective geological driving forces, that is, pCO_2-dependent sources and sinks. The change of sodium concentration in seawater, $[Na^+]$, can be calculated as:

$$Ms_{ocean}(t)\frac{d[Na^+](t)}{dt} = F^{Na}_W + F^{Na}_{Exb} - F^{Na}_{Exr} - F^{Na}_{Exd} - F^{Na}_{EB} - F^{Na}_{NAH} - F^{Na}_{RW}. \quad (19)$$

In equation (19), F_W^{Na} represents sodium influx from silicate weathering, parameterized as $F_W^{Na}(t_p)f_W$, where $F_W^{Na}(t_p)$ denotes the modern sodium weathering flux and f_W accounts for weathering enhancement due to rain pH. Here, $f_W = ((pCO_2K_HK_{A1})^{0.5}/[H^+]_{rain}(t_p))^{n_W}$, where $[H^+]_{rain}(t_p)$ represents the present-day proton concentration in rainwater exposed to 280 ppm CO_2 and n_W is the rain pH dependence exponent. The term F_{Exb}^{Na}, F_{Exr}^{Na} and F_{Exd}^{Na} denote sodium exchange fluxes with boundary layer sediments, riverine particles and deep sediments, respectively. The F_{Exb}^{Na} is a source of sodium to seawater, which is held constant. The exchanges of sodium with riverine particles and deep sediments are sinks, which are proportional to their present-day values and the sodium concentration in the seawater. Thus, F_{Exr}^{Na} and F_{Exd}^{Na} are modelled as $F_{Exr}^{Na}(t_p)[Na^+](t)/[Na^+](t_p)$ and $F_{Exd}^{Na}(t_p)[Na^+](t)/[Na^+](t_p)$, respectively. The term F_{EB}^{Na} is the net burial flux of halite, which is calculated as $F_{EB}(t_p)([Na^+](t)/[Na^+](t_p))([Cl^-](t)/[Cl^-](t_p))$. The term F_{NAH}^{Na} is a sodium sink during near-axis hydrothermal circulation, modelled as $F_{NAH}^{Na}(t_p)f_{NAH}[Na^+](t)/[Na^+](t_p)$, where $F_{NAH}^{Na}(t_p)$ is the present-day value and the factor f_{NAH} accounts for the enhancement of hydrothermal circulation due to higher heat flux on the early Earth. Lastly, the effect of reverse weathering on seawater sodium concentration is explored with F_{RW}^{Na}. The total amount of cations consumed during reverse weathering can be calculated as $F_{RW}(t_p)f_{RW}$, where $F_{RW}(t_p)$ is the present-day amount of total cations consumed, assuming an approximate 1:1 molar ratio of consumed silica to metal ions during reverse weathering reactions, and f_{RW} is a factor accounting for the relative intensities of reverse weathering compared to its present-day levels[39,40,75]. As $F_{RW}(t_p)$ accounts for all the cations consumed during reverse weathering (that is, Na^+, Mg^{2+} and K^+), F_{RW}^{Na} is parameterized as $F_{RW}(t_p)f_{RW}[Na^+](t)/([Na^+](t) + [Mg^{2+}](t) + [K^+](t))$. The values of the present-day carbon fluxes and the formulations of enhancement factors used in the model are summarized in Supplementary Table 2. It is noted that the sodium sink due to subduction of seawater is taken into account by the term Ms_{ocean}.

The seawater concentration of magnesium is tracked in a similar fashion to sodium, again following Halevy and Bachan[3]. The change of magnesium concentration in seawater, $[Mg^{2+}]$, can be calculated as:

$$Ms_{ocean}(t)\frac{d[Mg^{2+}](t)}{dt} = F_W^{Mg} + F_{GW}^{Mg} - F_{CB}^{Mg} - F_{NAH}^{Mg} - F_{OAH}^{Mg} - F_{RW}^{Mg}. \quad (20)$$

In equation (20), F_W^{Mg} represents magnesium influx from silicate weathering and is parameterized similarly to F_W^{Na}. The term F_{GW}^{Mg} represents the input of magnesium from ground water to ocean, which is assumed to be constant. The term F_{CB}^{Mg} denotes magnesium loss through carbonate burial, parameterized as $\frac{1}{2}F_{degas}^{C}(t_p)f_{degas}(f_D(t)/f_D(t_p))(f_{CARB}(t)/f_{CARB}(t_p))([Mg^{2+}](t)/[Mg^{2+}](t_p))$, where $F_{degas}^{C}(t_p)$ is the modern CO_2 degassing flux, f_{degas} is the mantle degassing enhancement factor, and f_D and f_{CARB} are the dolomite and carbonate fractions in buried carbonate, respectively. The terms F_{NAH}^{Mg} and F_{OAH}^{Mg} account for the magnesium sink due to near-axis and off-axis hydrothermal circulations, with $F_{NAH}^{Mg} = F_{NAH}(t_p)f_{NAH}\left([Mg^{2+}](t_p) - [Mg^{2+}]_{NAH}(t_p)\right)[Mg^{2+}](t)/[Mg^{2+}](t_p)$ and $F_{OAH}^{Mg} = F_{OAH}(t_p)f_{OAH}\left([Mg^{2+}](t_p) - [Mg^{2+}]_{OAH}(t_p)\right)[Mg^{2+}](t)/[Mg^{2+}](t_p)$. Here, $f_{NAH}(t_p)$ and $f_{OAH}(t_p)$ are the modern near-axis and off-axis water fluxes, f_{NAH} and f_{OAH} are the corresponding enhancement factors, and $[Mg^{2+}]_{NAH}(t_p)$ and $[Mg^{2+}]_{OAH}(t_p)$ are the modern concentrations of magnesium in near-axis and off-axis hydrothermal effluents. Finally, magnesium loss due to reverse weathering, F_{RW}^{Mg}, is parameterized similarly to F_{RW}^{Na}.

In our model, seawater concentrations of $[Cl^-]$, $[K^+]$ and $[SO_4^{2-}]$ are prescribed based on data from fluid inclusions in Archaean hydrothermal quartz[76], inferred halogen degassing history[77], and the sulfur isotopes found in both Archaean[78,79] and Palaeoproterozoic seawater sulfate reservoirs[80]. The Hadean $[Cl^-]$ is set to 1.87 times its present-day concentration (0.52 M)[76,77], whereas $[K^+]$ is estimated to be 40% of its present-day concentration (12.1 mM) from Earth's formation to 4 Ga (ref. 76; Extended Data Fig. 1e). These concentrations linearly transition to modern levels over 0.5 Gyr for $[Cl^-]$ and 1 Gyr for $[K^+]$, remaining constant thereafter. Potassium levels are then corrected according to different assumptions of reverse weathering. For Hadean and Archaean seawater, $[SO_4^{2-}]$ is estimated at 1–100 μM (refs. 78,79), and 0.1–5 mM for the Proterozoic[80].

On the other hand, the concentrations of $[HS^-]$, $[NH_4^+]$, $[Fe^{2+}]$ and $[Ca^{2+}]$ depend on the ocean pH and their equilibrium constants:

$$[HS^-] = \frac{K_{AS1}\sum S^{II-}}{K_{AS1} + [H^+]}, \quad (21)$$

$$[NH_4^+] = \frac{K_N[H^+]\sum N^{III-}}{1 + K_N[H^+]}, \quad (22)$$

$$[Fe^{2+}] = \frac{[H^+]\sum Fe^{II}}{K_{FeS}[HS^-] + [H^+]}, \quad (23)$$

$$[Ca^{2+}] = \frac{2n_{sat}K_{SP}[H^+]^4}{pCO_2K_HK_{A1}K_{A2}}, \quad (24)$$

where K_{AS1}, K_N and K_{FeS} are the first acid dissociation constant of H_2S, ammonium dissociation constant and FeS solubility product constant, respectively (Supplementary Table 1). These ion concentrations, however, are in turn necessary to solve for the ocean charge balance (equation (18)). Thus, knowing the total concentrations of ΣS^{II-}, ΣN^{III-} and ΣFe^{II} (ref. 3), we calculate the concentrations of $[HS^-]$, $[NH_4^+]$, $[Fe^{2+}]$ and $[Ca^{2+}]$ based on an initial $[H^+]$ value, iterating until convergence is reached for $[H^+]$ via charge balance. Because the concentrations of reduced species (ΣS^{II-}, ΣN^{III-} and ΣFe^{II}) are too low to affect seawater charge balance[3] (Extended Data Fig. 1b–d), they are assumed constant over time.

Combining the carbon cycle and ocean charge balance models, we have two unknowns, pCO_2 and $[H^+]$, solved by equations (16) and (18). We solve these equations forward in time using the following steps. First, we calculate major ion concentrations in seawater based on their geological drivers or dissociation constants, assuming an initial $[H^+]$ concentration. Second, we track the sizes of carbon reservoirs using equations (1)–(3). Third, the pCO_2 and ocean pH are calculated using equations (16) and (18). Lastly, we calculate the Earth's surface properties dependent on pCO_2 and/or seawater $[H^+]$, for example, seawater ion concentrations, carbon reservoir sizes and surface temperature.

The concentrations of $[HS^-]$, $[NH_4^+]$, $[Fe^{2+}]$ and $[Ca^{2+}]$ are calculated using ocean pH, pCO_2 and their dissociation equilibrium constants. Knowing the partial pressure of CO_2 in the atmosphere, the reservoir sizes of the atmosphere and oceans are obtained using equations (12) and (14), respectively.

A hybrid atmospheric model

The Earth's surface temperature is determined using a hybrid atmospheric model. When pCO_2 falls within the range of present-day value to 10 atm, the surface temperature is calculated utilizing a 1D radiative convective climate model[4]:

$$\begin{aligned} T(t) = {} & 3,145.89 - 894.196x - 14,231.92y - 3,791.699x^2 + 18,527.77x^2y \\ & -33,560.74x^2y^2 + 26,297.61y^2 - 7,674.76xy^2 + 4,461.16xy \\ & -1,569.25x^3 + 11,329.25x^3y^3 - 21,270.62y^3 - 14,022.32x^3y^2 \\ & +26,860.83x^2y^3 + 7,684.55x^3y + 5,722.64xy^3 - 178.264x^4 \\ & -396.147x^4y^4 + 6,399.091y^4 + 875.423x^4y - 1,605.364x^4y^2 \\ & +1,304.944x^4y^3 - 1,569.3007xy^4 - 8,012.67x^2y^4 - 3,415.93x^3y^4, \end{aligned} \quad (25)$$

where x represents $\log_{10}(pCO_2)$, where pCO_2 is in bar and y represents the relative solar irradiance compared to present-day level. We assume that the solar irradiance has linearly increased from 952 W m^{-2} at the beginning of Earth history to 1,360 W m^{-2} at present day. In this model, the albedo is assumed to be 0.32. A Manabe–Wetherald relative humidity model is applied to the troposphere[81], with a surface relative humidity of 0.8.

When pCO_2 exceeds 10 atm, the temperature is determined employing a two-layer grey atmosphere model, following ref. 82 and ref. 42. This shift of modelling strategy is necessary as the 10 atm exceeds the upper limit tested by the polynomial fit conducted in the 1D model and the application of grey atmosphere assumption is inappropriate at low pCO_2 conditions. In this model, the Earth's surface temperature is calculated by first establishing physical conditions at the tropopause based on radiation balance and a specified water vapour mixing ratio, q. Second, using the temperature and optical depth at the tropopause as reference, the thermal structures of the stratosphere and troposphere are determined by applying energy balance and the moist adiabatic lapse rate, respectively. Finally, a bisection search adjusts q to maintain energy balance at the top of the atmosphere, with the temperature at the bottom of the troposphere representing the Earth's surface temperature. This model assumes a plane-parallel atmosphere that is transparent to solar radiation and opaque to infrared radiation at all wavelengths, with a constant absorption coefficient for infrared radiation[42,82].

The values of the initial Earth conditions used in the model, including the concentrations of seawater ions and the carbon reservoirs sizes, are summarized in Supplementary Table 2.

Data availability

Source data are available at https://doi.org/10.6084/m9.figshare.28172345.v1 (ref. 83).

Code availability

The MATLAB codes are available at https://doi.org/10.24433/CO.2739452.v3 (ref. 84).

References

54. Sleep, N. H., Zahnle, K. J. & Lupu, R. E. Terrestrial aftermath of the Moon-forming impact. *Phil. Trans. R. Soc. A* **372**, 20130172 (2014).
55. Korenaga, J. Was there land on the early Earth? *Life* **11**, 1142 (2021).
56. Driscoll, P. & Bercovici, D. Divergent evolution of Earth and Venus: influence of degassing, tectonics, and magnetic fields. *Icarus* **226**, 1447–1464 (2013).
57. Tajika, E. & Matsui, T. Evolution of terrestrial proto-CO_2 atmosphere coupled with thermal history of the earth. *Earth Planet. Sci. Lett.* **113**, 251–266 (1992).
58. Galvez, M. E. & Pubellier, M. in *Deep Carbon: Past to Present* (eds Orcutt, B. N., Daniel, I. & Dasgupta, R.) 276–312 (Cambridge Univ. Press, 2019).
59. Berner, R. A., Lasaga, A. C. & Garrels, R. M. Carbonate–silicate geochemical cycle and its effect on atmospheric carbon dioxide over the past 100 million years. *Am. J. Sci.* **283**, 641–683 (1983).
60. Brady, P. V. The effect of silicate weathering on global temperature and atmospheric CO_2. *J. Geophys. Res. Solid Earth* **96**, 18101–18106 (1991).
61. Gaillardet, J., Dupré, B., Louvat, P. & Allegre, C. J. Global silicate weathering and CO_2 consumption rates deduced from the chemistry of large rivers. *Chem. Geol.* **159**, 3–30 (1999).
62. Klaminder, J. et al. Silicate mineral weathering rate estimates: are they precise enough to be useful when predicting the recovery of nutrient pools after harvesting? *For. Ecol. Manage.* **261**, 1–9 (2011).
63. Moon, S., Chamberlain, C. P. & Hilley, G. E. New estimates of silicate weathering rates and their uncertainties in global rivers. *Geochim. Cosmochim. Acta* **134**, 257–274 (2014).
64. White, A. F. & Brantley, S. L. (eds) *Chemical Weathering Rates of Silicate Minerals* Vol. 31 (De Gruyter, 2018).
65. Kasting, J. F., Pollack, J. B. & Ackerman, T. P. Response of Earth's atmosphere to increases in solar flux and implications for loss of water from Venus. *Icarus* **57**, 335–355 (1984).
66. Taboada, T., Rodríguez-Lado, L., Ferro-Vázquez, C., Stoops, G. & Cortizas, A. M. Chemical weathering in the volcanic soils of Isla Santa Cruz (Galápagos Islands, Ecuador). *Geoderma* **261**, 160–168 (2016).
67. Mills, B., Lenton, T. M. & Watson, A. J. Proterozoic oxygen rise linked to shifting balance between seafloor and terrestrial weathering. *Proc. Natl Acad. Sci. USA* **111**, 9073–9078 (2014).
68. Brady, P. V. & Gíslason, S. R. Seafloor weathering controls on atmospheric CO_2 and global climate. *Geochim. Cosmochim. Acta* **61**, 965–973 (1997).
69. Nakamura, K. & Kato, Y. Carbonatization of oceanic crust by the seafloor hydrothermal activity and its significance as a CO_2 sink in the Early Archean. *Geochim. Cosmochim. Acta* **68**, 4595–4618 (2004).
70. Gillis, K. M. & Coogan, L. A. Secular variation in carbon uptake into the ocean crust. *Earth Planet. Sci. Lett.* **302**, 385–392 (2011).
71. Fischer, T. P. Fluxes of volatiles (H_2O, CO_2, N_2, Cl, F) from arc volcanoes. *Geochem. J.* **42**, 21–38 (2008).
72. Van Der Meer, D. G. et al. Plate tectonic controls on atmospheric CO_2 levels since the Triassic. *Proc. Natl Acad. Sci. USA* **111**, 4380–4385 (2014).
73. Kerrick, D. M. Present and past nonanthropogenic CO_2 degassing from the solid Earth. *Rev. Geophys.* **39**, 565–585 (2001).
74. Brune, S., Williams, S. E. & Müller, R. D. Potential links between continental rifting, CO_2 degassing and climate change through time. *Nat. Geosci.* **10**, 941–946 (2017).
75. Krissansen-Totton, J. & Catling, D. C. A coupled carbon–silicon cycle model over Earth history: reverse weathering as a possible explanation of a warm mid-Proterozoic climate. *Earth Planet. Sci. Lett.* **537**, 116181 (2020).
76. Marty, B., Avice, G., Bekaert, D. V. & Broadley, M. W. Salinity of the Archaean oceans from analysis of fluid inclusions in quartz. *C. R. Géosci.* **350**, 154–163 (2018).
77. Guo, M. & Korenaga, J. A halogen budget of the bulk silicate Earth points to a history of early halogen degassing followed by net regassing. *Proc. Natl Acad. Sci. USA* **118**, e2116083118 (2021).
78. Jamieson, J. W., Wing, B. A., Farquhar, J. & Hannington, M. D. Neoarchaean seawater sulphate concentrations from sulphur isotopes in massive sulphide ore. *Nat. Geosci.* **6**, 61–64 (2012).
79. Crowe, S. A. et al. Sulfate was a trace constituent of Archean seawater. *Science* **346**, 735–739 (2014).
80. Scott, C. et al. Pyrite multiple-sulfur isotope evidence for rapid expansion and contraction of the early Paleoproterozoic seawater sulfate reservoir. *Earth Planet. Sci. Lett.* **389**, 95–104 (2014).
81. Manabe, S. & Wetherald, R. T. Thermal equilibrium of the atmosphere with a given distribution of relative humidity. *J. Atmos. Sci.* **24**, 241–259 (1967).
82. Nakajima, S., Hayashi, Y. Y. & Abe, Y. A study on the 'runaway greenhouse effect' with a one-dimensional radiative–convective equilibrium model. *J. Atmos. Sci.* **49**, 2256–2266 (1992).
83. Guo, M. & Korenaga, J. out_phase3_scenario1.dat. *Figshare* https://doi.org/10.6084/m9.figshare.28172345.v1 (2025).
84. Guo, M. & Korenaga, J. Rapidly evolving ocean pH in the early Earth: insights from global carbon cycle coupled with ocean chemistry. *Code Ocean* https://doi.org/10.24433/CO.2739452.v3 (2025).

Acknowledgements

This article was based on work supported by NASA astrobiology grant no. 80NSSC19M0069 (J.K.) and Nanyang Technological University Presidential Postdoctoral Fellowship 023878-00001 (M.G.).

Author contributions

M.G. performed the modelling and wrote the paper. J.K. designed the project, discussed the results and commented on the paper.

Competing interests
The authors declare no competing interests.

Additional information
Extended data is available for this paper at https://doi.org/10.1038/s41561-025-01649-9.

Supplementary information The online version contains supplementary material available at https://doi.org/10.1038/s41561-025-01649-9.

Correspondence and requests for materials should be addressed to Meng Guo.

Peer review information *Nature Geoscience* thanks Nick Arndt, Terry Isson and Shintaro Kadoya for their contribution to the peer review of this work. Primary Handling Editor: Alison Hunt, in collaboration with the *Nature Geoscience* team.

https://doi.org/10.1038/s41561-025-01649-9

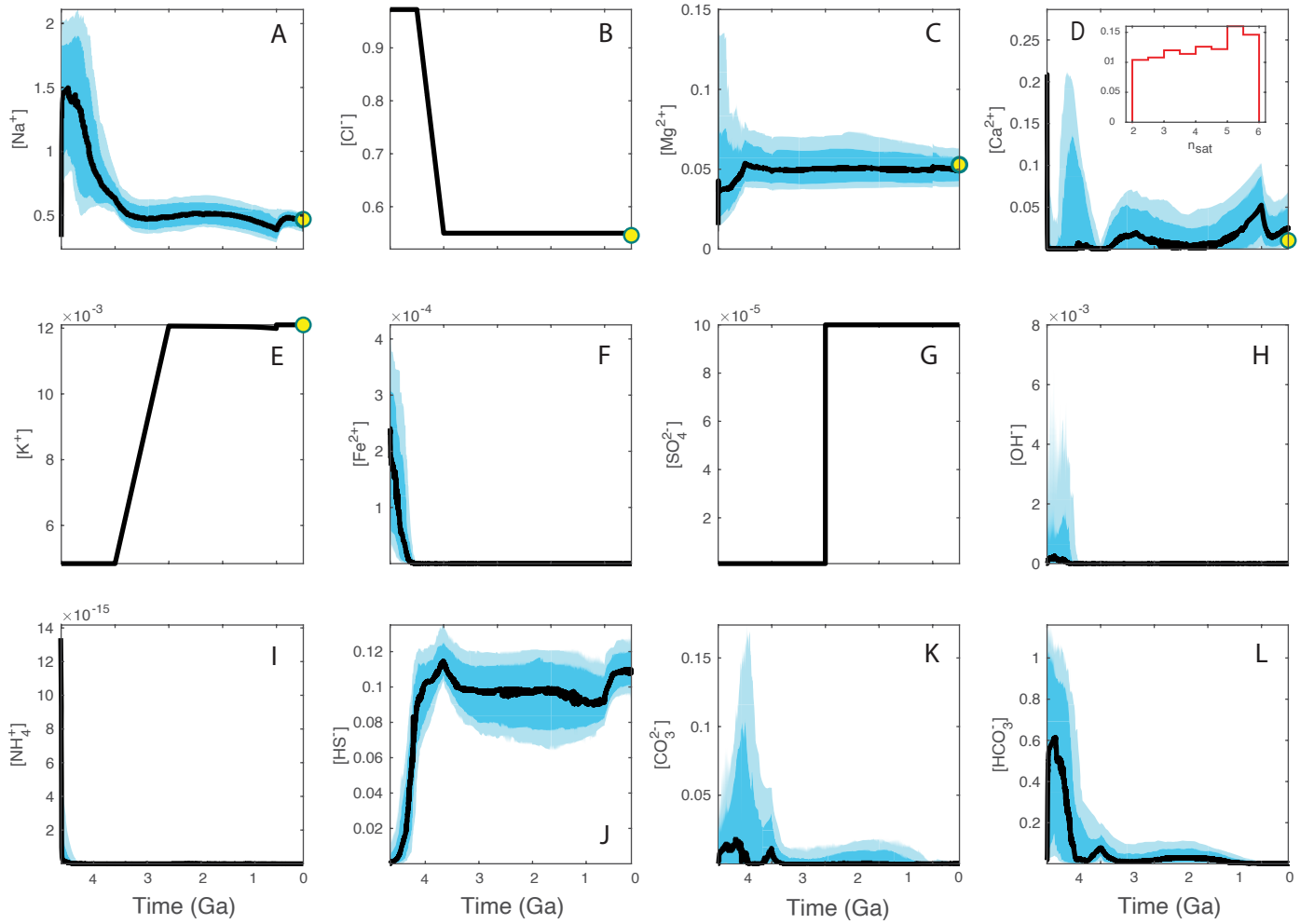

Extended Data Fig. 1 | Successful model solutions and observational constraints of seawater ion concentrations. Constraints used to select solutions are shown in yellow[37]. The mid-50% and mid-90% ranges of successful solutions are shown in dark blue and light blue, respectively, with solid lines indicating the medians. A total of 145 successful solutions were analyzed. (**a-l**) Evolutions of seawater concentration of $[Na^+]$, $[Cl^-]$, $[Mg^{2+}]$, $[Ca^{2+}]$, $[K^+]$, $[Fe^{2+}]$, $[SO_4^{2-}]$, $[OH^-]$, $[NH_4^+]$, $[HS^-]$, $[CO_3^{2-}]$, and $[HCO_3^-]$, respectively. The posterior distribution of $CaCO_3$ saturation factor in oceans is shown as an inset within panel (D).

https://doi.org/10.1038/s41561-025-01649-9

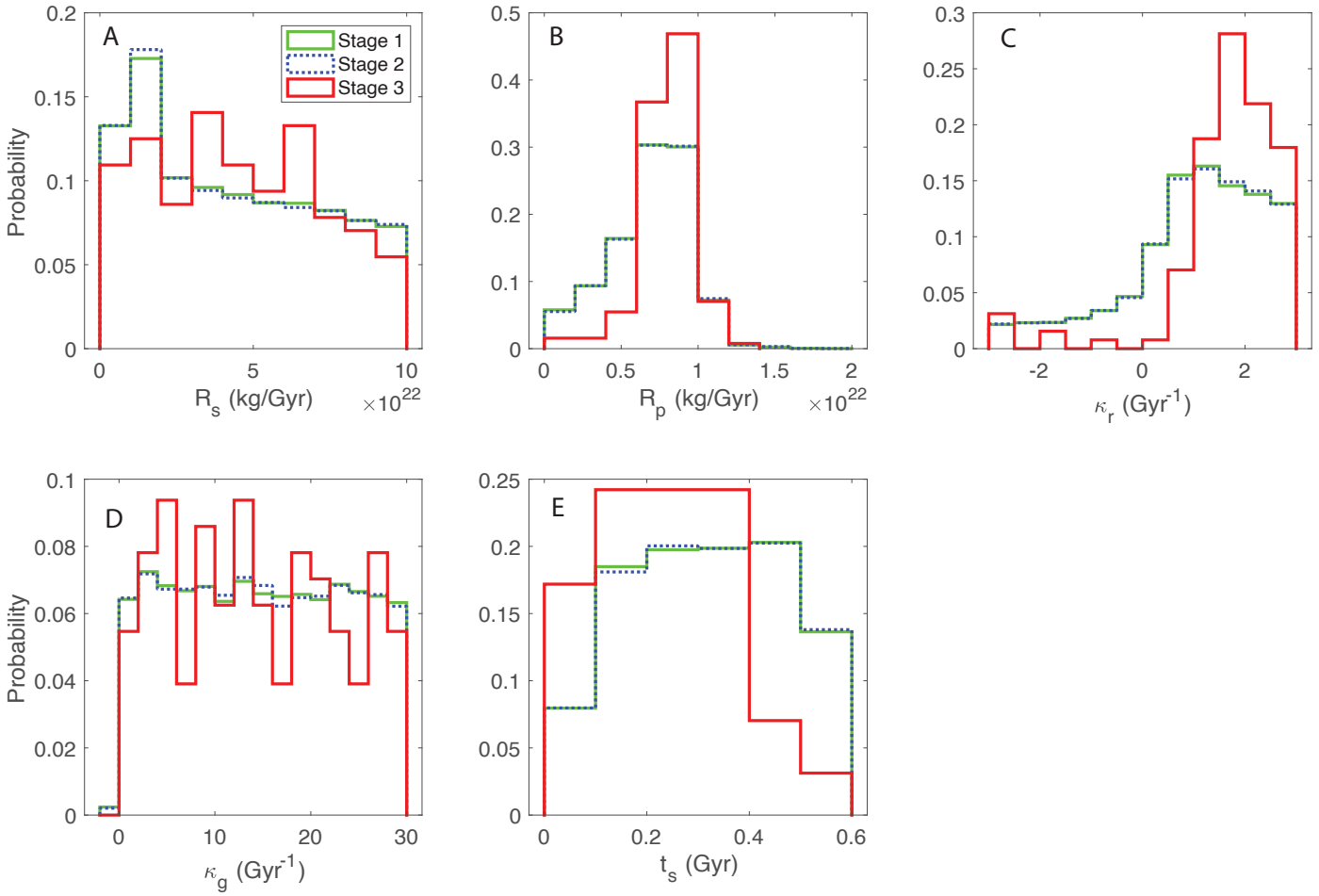

Extended Data Fig. 2 | A posteriori distributions of crustal evolution parameters, based on ~300, ~300, and 145 successful Monte Carlo solutions from stages 1, 2, and 3, respectively. Distributions from stages 1, 2, and 3 are shown in green, blue, and red, respectively. (**a**) Initial recycling rate, (**b**) present-day recycling rate, (**c**) decay constant for crustal recycling, (**d**) decay constant for crustal generation, and (**e**) onset time for crustal formation.

https://doi.org/10.1038/s41561-025-01649-9

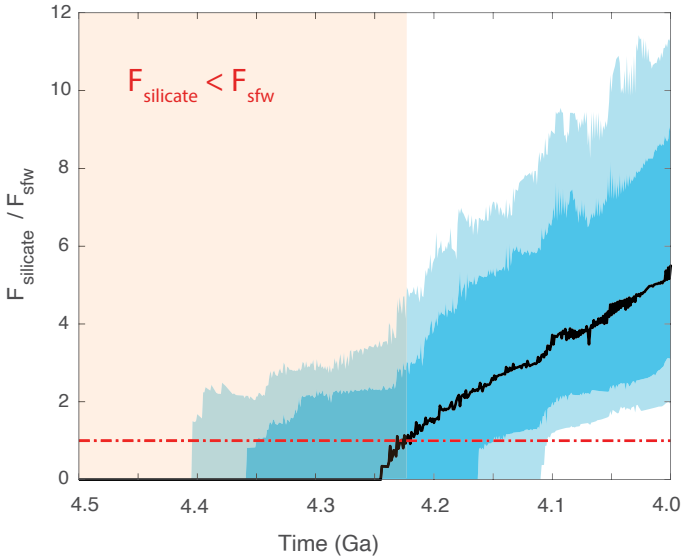

Extended Data Fig. 3 | The ratio of silicate weathering rate to seafloor weathering rate during the Hadean. The mid-50% and mid-90% ranges of successful solutions are shown in dark blue and light blue, respectively, with solid lines indicating the medians. A total of 145 successful solutions were analyzed. The dashed line is drawn at 1 ($F_{silicate} = F_{sfw}$). The orange-shaded area represents periods when the seafloor weathering rate exceeds the silicate weathering rate.

https://doi.org/10.1038/s41561-025-01649-9

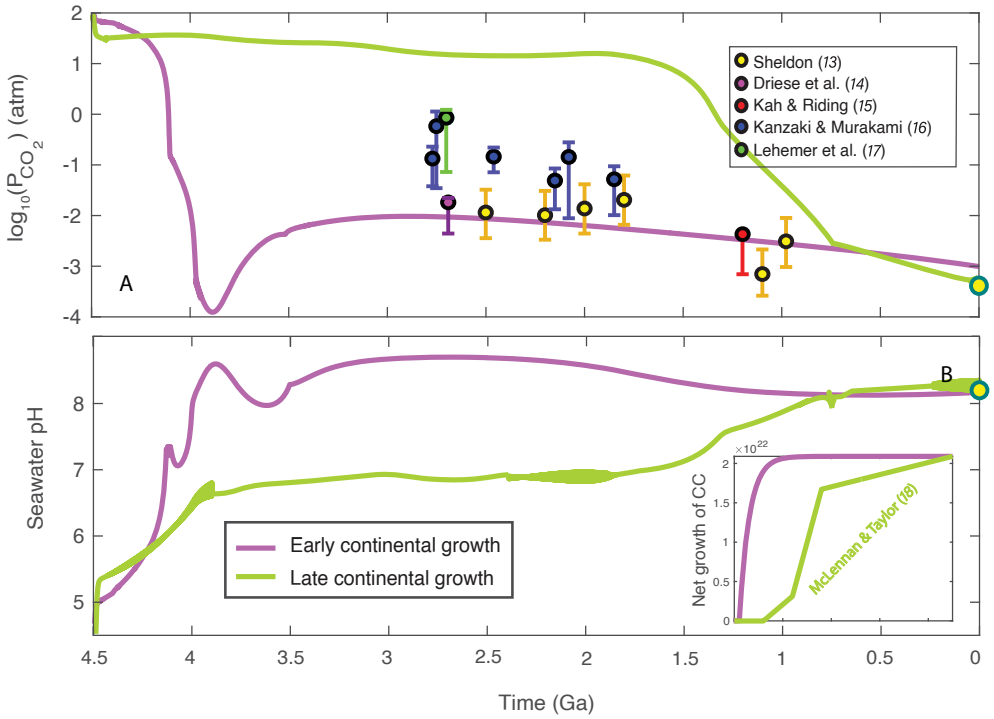

Extended Data Fig. 4 | The model solutions and observational constraints, with early- and late-growth of continental crust. Constraints used to select solutions are shown by colored circles, and the error bars represent 2 standard deviations. (**a**) The pCO_2 with proxies from the literature[13–17]. (**b**) Ocean pH. The continental formation models used for the early- and late-growth scenarios of continental crust are shown as insets in panel (B). For the model of McLennan and Taylor[18], we assume that the recycling rate of continental crust remains constant over time.